


Review

Application of Heterogeneous Catalysis in Formic Acid-Based Hydrogen Cycle System

Zhenzhen Wang, Junfeng Qian *, Zhonghua Sun, Zhihui Zhang , Mingyang He * and Qun Chen

Jiangsu Key Laboratory of Advanced Catalytic Materials and Technology, Advanced Catalysis and Green Manufacturing Collaborative Innovation Center, Changzhou University, Changzhou 213164, China; wangzhenzhen@cczu.edu.cn (Z.W.)

* Correspondence: qianjunfeng@cczu.edu.cn (J.Q.); hmy@cczu.edu.cn (M.H.)

Abstract: H₂ has aroused significant attention as an unpolluted and renewable energy carrier. However, the efficient storage and controllable release of H₂ are urgent to be addressed. Through the hydrogenation of CO₂ (bicarbonate) to produce formic acid (formate) and reverse dehydrogenation reactions, a carbon-neutral formic acid-based hydrogen cycle system can be established. Given the excellent recyclability and facile separation of heterogeneous catalysis, the development of heterogeneous catalysts for these reversible interconversions is thoroughly summarized, with a special focus on the structure–activity relationship and the mechanistic insight. Finally, the challenges and opportunities surrounding the formic acid-based hydrogen cycle system are discussed. It is hoped that this review will provide guidance and an idea for the design and development of efficient heterogeneous catalysts for the carbon-neutral H₂ storage and release system.

Keywords: heterogeneous catalysis; hydrogen cycle system; supported catalyst; hydrogenation; dehydrogenation



Citation: Wang, Z.; Qian, J.; Sun, Z.; Zhang, Z.; He, M.; Chen, Q. Application of Heterogeneous Catalysis in Formic Acid-Based Hydrogen Cycle System. *Catalysts* **2023**, *13*, 1168. <https://doi.org/10.3390/catal13081168>

Academic Editor: Giuseppe Bonura

Received: 29 June 2023

Revised: 26 July 2023

Accepted: 27 July 2023

Published: 30 July 2023



Copyright: © 2023 by the authors. Licensee MDPI, Basel, Switzerland. This article is an open access article distributed under the terms and conditions of the Creative Commons Attribution (CC BY) license (<https://creativecommons.org/licenses/by/4.0/>).

1. Introduction

With high gravimetric specific energy (33.3 kW·h/kg) and zero pollution during combustion, H₂ has been considered the most promising energy carrier in a low-carbon economy [1–3]. However, due to its low volumetric energy density (2.5 W·h/L) and flammability, it still faces some challenges as an energy carrier in actual storage and transportation [4–7]. To effectively store and transport H₂, various approaches have been developed [8–11]. Among them, liquid organic hydrogen carriers (LOHCs), such as formic acid (FA) [12–15], methanol (CH₃OH) [16–18], ammonia borane (NH₃BH₃) [19–22], and hydrazine hydrate (N₂H₄·H₂O) [23–25], have gained widespread attention in recent years because of their high hydrogen content, easy storage, and transportation.

As a typical LOHC, FA is supposed to be a promising H₂ storage material with a high volumetric hydrogen density (53 g/L) [26–28]. In addition, FA is low toxic, nonflammable, and liquid under ambient conditions, which is convenient to store and transport [29–33]. Moreover, compared with other LOHCs, FA can easily dehydrogenate to release H₂ and can be regenerated under relatively mild conditions [34–37]. At present, the most prominent FA production process is methyl formate hydrolysis, but the use of high-concentration CO for the carbonylation process of methanol poses potential safety hazards [38]. Alternatively, catalytic hydrogenation of CO₂ to produce FA (CO₂ + H₂ → HCOOH) with 100% atomic efficiency can not only achieve efficient storage of hydrogen energy but also effectively reduce carbon emissions and synthesize high-value-added chemicals, attracting increasing interest [39–44]. H₂ chemically sealed in FA can be easily retrieved on-demand under mild conditions [45–49], which constitutes a promising carbon-neutral and environmentally benign FA-based hydrogen cycle system (Figure 1).

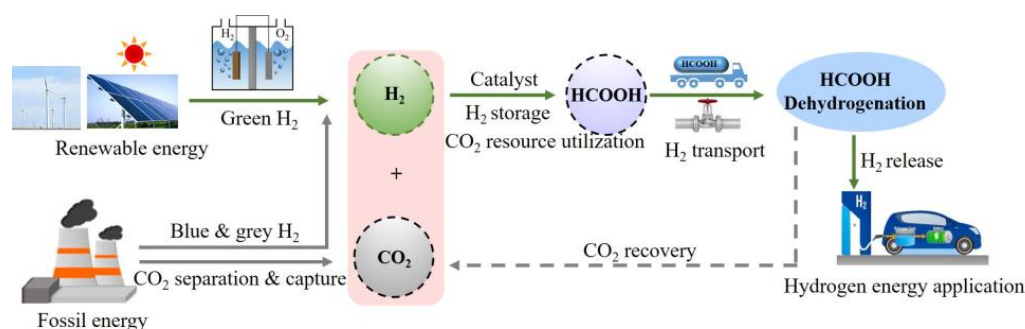


Figure 1. Carbon-neutral FA-based hydrogen cycle system.

Unfortunately, the direct catalytic hydrogenation of gaseous CO_2 to FA ($\text{CO}_2 + \text{H}_2 \rightarrow \text{HCOOH}$, $\Delta_r G^\circ_{298\text{K}} = +32.9 \text{ kJ/mol}$) is thermodynamically adverse because of its high chemical stability [50,51]. If the reaction is carried out in an aqueous solution, negative free energy ($\Delta_r G^\circ_{298\text{K}} = -4 \text{ kJ/mol}$) will be obtained due to the dissolution of the reaction gas [52,53]. An even stronger exergonic trend ($\Delta_r G^\circ_{298\text{K}} = -35 \text{ kJ/mol}$) will be observed if an alkaline aqueous solution is used [54,55]. Here, the generated FA is captured by the base in FA-base adducts form, which benefits a rightward shift of the reaction equilibrium. On the other hand, the H_2 release process from FA ($\text{HCOOH} \rightarrow \text{CO}_2 + \text{H}_2$, $\Delta_r G^\circ_{298\text{K}} = -32.9 \text{ kJ/mol}$) is the reverse reaction of CO_2 hydrogenation to FA, which can proceed readily with favorable thermodynamics [56–58]. Compared to CO_2 molecules, the hydrogenation of bicarbonate can proceed under much milder conditions, so a formate/bicarbonate salt-based reversible H_2 storage couple is also attractive [59–66].

Although substantial progress has been achieved for CO_2 (bicarbonate) hydrogenation and FA (formate) dehydrogenation, and a large number of outstanding reviews on homogeneous and heterogeneous catalytic systems have emerged [67–73], the hydrogenation and dehydrogenation processes are generally studied individually on different catalysts suitable for each reaction. It is highly desired to develop a catalyst that can concomitantly catalyze the hydrogenation and dehydrogenation processes for a hydrogen cycle system. Although homogeneous catalysts exhibit superior catalytic activity, disadvantages, such as the use of expensive ligands and inseparability from the catalytic system, seriously restrict their industrial applications [74–77]. In contrast, heterogeneous catalysts possess significant advantages in product separation, recycling, and continuous operation, providing prospects for their industrial applications [78–82]. Accordingly, this review focuses on and summarizes recent progress in the reaction system of heterogeneous catalysis for the interconversion between CO_2 (bicarbonate) and FA (formate) over the same catalyst, from the first example through the most recent advancement in early 2023. By summarizing the results obtained from these studies, we hope to provide some valuable references to the development of a highly efficient heterogeneous catalyst, ultimately making the hydrogen cycle system more practical. The challenges and opportunities worthy of further research for the FA-based hydrogen cycle system are proposed.

2. Heterogeneous Catalysis in FA-based Hydrogen Cycle System

2.1. Monometal-Based Heterogeneous Catalytic System

2.1.1. Activated Carbon-Supported Monometallic Catalysts

In 1986, Sasson and co-workers proposed that the cyclic transformation of formate/bicarbonate was promising for H_2 storage and transport [83]. Three years later, they first reported the use of a heterogeneous catalyst (Pd/C) for the reversible conversion between formate (50°C , 1 atm) and bicarbonate (30°C , 5 atm) [84].

Considering the good solubility of ammonium formate (NH_4HCO_2) and thus improved volumetric hydrogen density, Lin et al. reported an ammonium bicarbonate (NH_4HCO_3)/ NH_4HCO_2 -based reversible H_2 storage-release system over a Pd/AC catalyst in 2015 [85]. The reaction pressure and temperature are critical factors governing

the switch between H_2 storage and the release steps in the same catalytic system. For the hydrogenation process, up to a 96% yield of NH_4HCO_2 with a corresponding TOF of 118 h^{-1} (20°C , 2.75 MPa H_2) was achieved, whereas a 92% hydrogen yield with a TOF of 1132 h^{-1} (80°C , 0.1 MPa N_2) was obtained from the dehydrogenation of NH_4HCO_2 . The main by-products were CO_2 and NH_3 generated from the decomposition of NH_4HCO_3 and NH_4HCO_2 at an elevated reaction temperature (an increase from 20 to 120°C). In 2018, the same research group also used Pd/AC to catalyze reversible CO_2 hydrogenation and formate dehydrogenation reactions under mild operating conditions [86]. It was found that piperidine added in the reversible reaction system acted as a reactant trap, promoting the CO_2 hydrogenation and formate dehydrogenation processes. Furthermore, a significant solvent-promoting effect was observed in the reversible process. In a 70% ethanol aqueous solution, a 96% yield of formate was achieved during a hydrogenation reaction at 30°C , and the TOF value was as high as 5945 h^{-1} ; for the formate dehydrogenation process, the yield of H_2 reached 92.1%, with a $\text{TOF}_{\text{initial}}$ of 9908 h^{-1} at 100°C . Additionally, the mechanism study showed that the existence of piperidine tailored the electronic property of Pd and reduced the free energy of the hydrogenation and dehydrogenation processes, further resulting in improved catalytic activity for the reversible H_2 storage and release cycle. Notably, the Pd/AC catalyst possessed excellent stability, with negligible activity decline in the five hydrogenation–dehydrogenation cycling tests.

2.1.2. Mesoporous Carbon-Supported Monometallic Catalysts

Furthermore, in 2016, Cao and colleagues found that electron-rich pyridinic-N-doped carbon hybrids (CNs) could effectively regulate the electronic property of a Pd catalyst, thus ameliorating its catalytic activity for reversible conversion between FA and CO_2 [87]. CN materials with different N/C molar ratios were prepared by pyrolysis of chitosan and melamine, which acted as a sturdy support to anchor uniformly dispersed Pd NPs ($3.1 \pm 0.3 \text{ nm}$). Figure 2 presents a positive linear correlation between FA dehydrogenation activity and the molar ratio of pyridinic-N/Pd, suggesting that the surface pyridinic-N strongly altered the electronic property of Pd, thus promoting its catalytic performance. The optimized Pd/CN_{0.25} catalyst displayed excellent activity for FA dehydrogenation and CO_2 hydrogenation, with TOF values of 5530 h^{-1} (25°C) and 1837 h^{-1} (100°C), respectively.

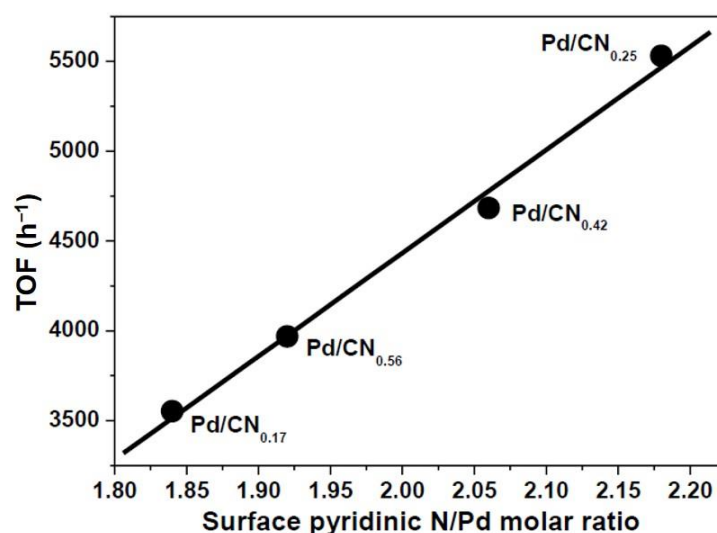


Figure 2. Correlation between molar ratio of surface pyridinic N/Pd and $\text{TOF}_{\text{initial}}$ value with Pd/CN_x catalysts. Reprinted with permission from Ref. [87]. Copyright 2016, Wiley.

Huang and Zhang et al. established a carbon-neutral hydrogen cycle system based on $\text{KHCO}_3/\text{HCOOK}$ redox equilibrium in 2016, which was catalyzed by Pd NPs anchored by N-doped mesoporous carbon [88]. The activity of Pd/NMC for either the hydrogenation of KHCO_3 or H_2 release from HCOOK was superior to that of nitrogen-free Pd/MC, indicating

that the doped N-containing functionalities played a vital role in the interconversion of KHCO_3 and HCOOK . The experimental and characterization results showed that the N-containing functionalities in Pd/NMC inhibited the aggregation of Pd NPs, increased the electron density of the Pd element, and promoted the absorption of HCO_3^- and HCOO^- through electrostatic interaction (Figure 3a–g), which synergistically facilitated the hydrogenation of KHCO_3 (799 h^{-1} at 80°C) and the dehydrogenation of HCOOK (1118 h^{-1} at 60°C). As shown in Figure 3g, they proposed a reaction mechanism for the reversible H_2 storage and release process on Pd/NMC. For the hydrogenation of HCO_3^- , Pd NPs catalyzed the dissociation of H_2 , forming Pd–H species. Then, the resulting Pd–H species attacked the C–OH bonds of HCO_3^- , forming HCOO^- and OH^- . Finally, the formed OH^- combined with the remaining H absorbed by the Pd NPs to release H_2O . For the dehydrogenation of HCOO^- , the Pd NPs facilitated the release of CO_2 by adsorption of H from the cleavage of C–H bonds in the HCOO^- . The H absorbed by the Pd NPs was then combined with the H produced by the O–H bond breaking of H_2O to form H_2 .

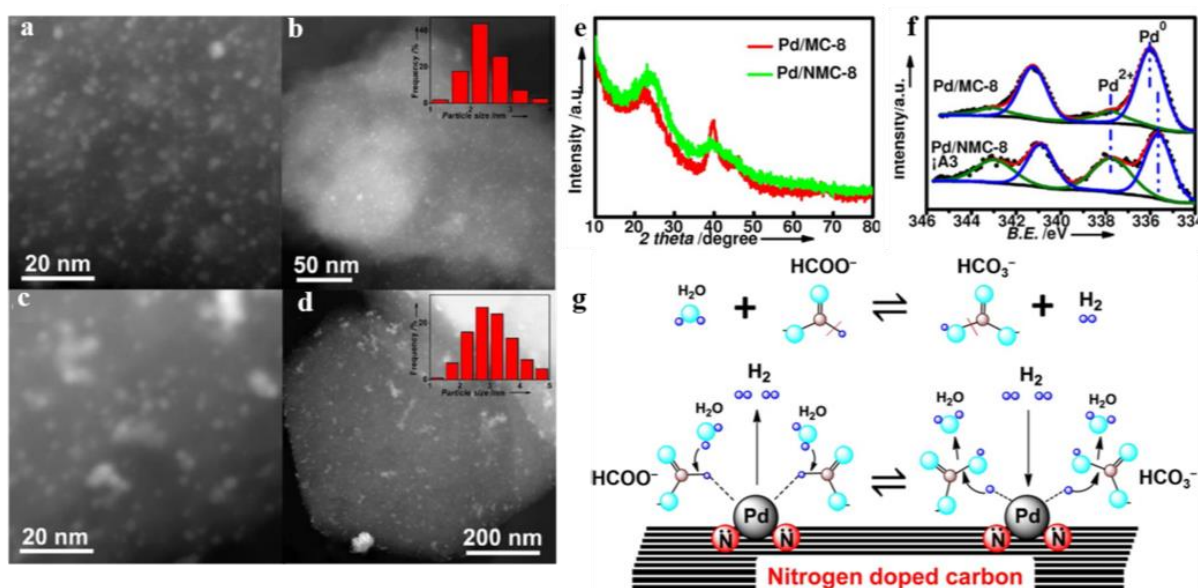


Figure 3. STEM images of (a,b) Pd/NMC-8 and (c,d) Pd/MC-8. (e) XRD patterns and (f) Pd 3d XPS spectra of Pd/MC-8 and Pd/NMC-8. (g) Probable reaction mechanisms for formate dehydrogenation and bicarbonate hydrogenation over Pd/NMC. Reprinted with permission from Ref. [88]. Copyright 2016, Wiley.

In 2017, Asefa, Yoon, et al. synthesized polyaniline-derived N-doped mesoporous carbon (PDMC) through a hard template method coupled with pyrolysis to immobilize Pd NPs [89]. The preparation process of the Pd/PDMC nanocatalyst is shown in Figure 4a. The catalytic performance of the as-obtained Pd/PDMC for the reversible transformation between NaHCO_2 and NaHCO_3 was found to be dependent on the dosage of the hard template and pyrolysis temperature (Figure 4b–e). With an increasing hard template dosage, the specific surface area and porosity enlarged markedly. Thanks to the large surface areas, high porosity, and a large number of electron-rich N-containing functionalities in the PDMC, the optimized Pd/PDMC catalyst exhibited good activity for H_2 release from NaHCO_2 ($\text{TOF} = 2562 \text{ h}^{-1}$) and NaHCO_3 hydrogenation ($\text{TOF} = 68 \text{ h}^{-1}$) at 80°C .

In 2020, Shao, Ji, et al. prepared N,P-co-doped porous carbon through the pyrolysis of a 1,10-phenanthroline and triphenylphosphine mixture to immobilize Pd NPs [90]. The resulting Pd/N,P-C catalyst displayed good catalytic performance for H_2 generation from HCOOK ($\text{TOF} = 3248 \text{ h}^{-1}$, 80°C) and KHCO_3 hydrogenation ($\text{TOF} = 2805 \text{ h}^{-1}$, 80°C , 8 MPa H_2). DFT studies and XPS analysis revealed that the good activity of the Pd/N,P-C was ascribed to the electron-rich Pd, which was regulated by N- and P-containing electron-donating groups doped into the carbon support (Figure 5a–d). In addition, the Pd/N,P-

C showed good stability in five dehydrogenations and three hydrogenation reactions, respectively, and no deactivation was observed.

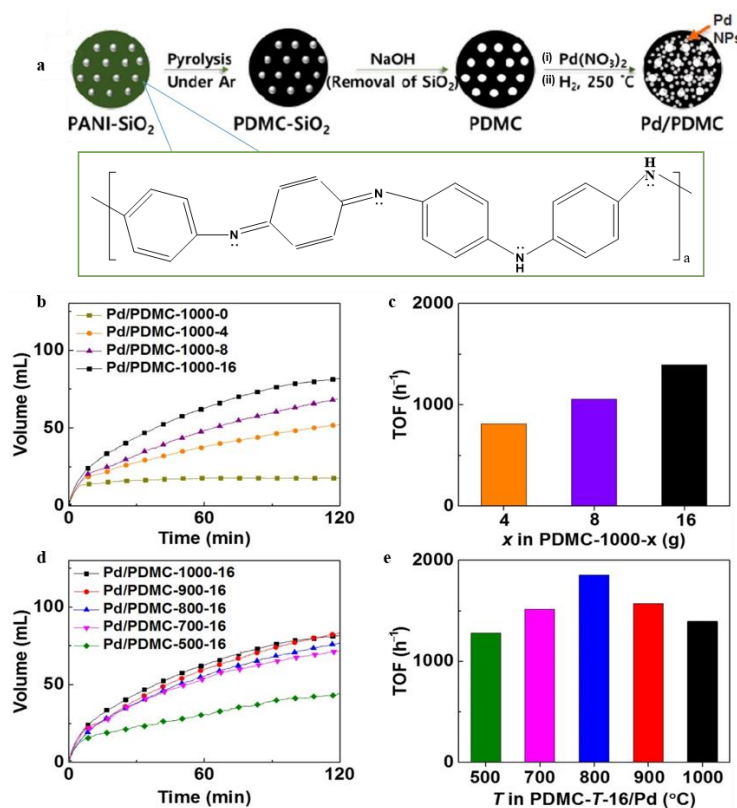


Figure 4. (a) Synthesis scheme of Pd/PDMC catalyst. The effects of (b,c) the amount of the hard template and (d,e) pyrolysis temperature on produced H₂ versus the reaction time and corresponding TOF values of NaHCO₂ dehydrogenation. Reproduced with permission from Ref. [89]. Copyright 2016, Elsevier.

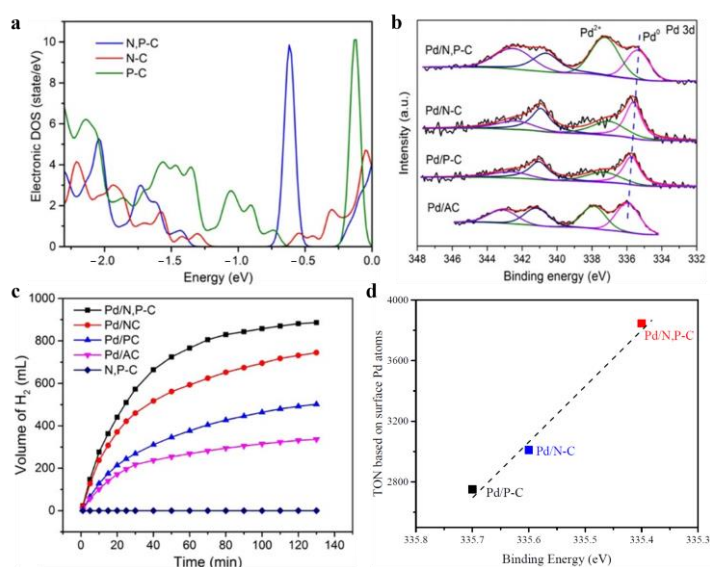


Figure 5. (a) Density of states (DOS) plots of various carbon-based materials. (b) Pd 3d XPS spectra of the catalysts supported by carbon-based materials. (c) Formate dehydrogenation activity catalyzed by different Pd-based catalysts at 80 °C. (d) Relation between the TON of bicarbonate hydrogenation and Pd 3d binding energy. Reaction conditions: 20 mg catalyst, 4 M bicarbonate aqueous solution, 6 MPa H₂, 80 °C. Reproduced with permission from Ref. [90]. Copyright 2020, American Chemical Society.

2.1.3. Graphite-Supported Monometallic Catalysts

Cao and co-workers reported that Pd NPs anchored by reduced graphite oxide (r-GO) could efficiently decompose a potassium formate (HCOOK) aqueous solution with a $\text{TOF}_{\text{initial}}$ of $11,299 \text{ h}^{-1}$ at 80°C [91]. Pd/r-GO can also catalyze the hydrogenation of potassium bicarbonate (KHCO_3) with a TOF of 242 h^{-1} at 100°C . The highly efficient H_2 charge/discharge over Pd/r-GO was ascribed to the lattice microstrain of Pd derived from the lattice mismatch between Pd and r-GO. As displayed in Figure 6a, a positive correlation between lattice expansion and dehydrogenation activity was identified. Noteworthy, they realized the reversible conversion of HCOOK and KHCO_3 in a single reaction vessel over the single catalyst (Pd/r-GO), indicating that a rechargeable formate-based H_2 storage system had been built. As shown in Figure 6b, the Pd/r-GO catalyst also showed long-term stability; the original HCOOK can be wholly decomposed after storing the catalyst-containing charged solution system under environmental conditions for 4 months. The Pd/r-GO catalyst also exhibited excellent recycling stability; six consecutive dehydrogenation and hydrogenation cycles were performed by controlling the reaction pressure and temperature (inset in Figure 6b).

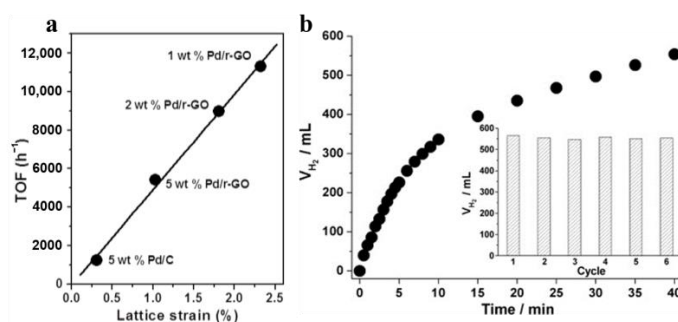


Figure 6. (a) Correlation between lattice strain and $\text{TOF}_{\text{initial}}$ value of FA dehydrogenation over Pd-based catalysts. (b) H_2 release process after charged solution stored for 4 months at 80°C . The inset demonstrates H_2 release (80°C) and storage (100°C , 4 MPa H_2) cycles over 1 wt% of Pd/r-GO. Reprinted with permission from Ref. [91]. Copyright 2014, Wiley.

In 2019, Lim's group elucidated the mechanism underlying the reversible transformation between HCO_3^- and HCO_2^- on a N-doped graphene-tethered Pd nanocluster (NC) by density functional theory (DFT) calculations [92]. As indicated in Figure 7a–h, the rate-determining steps for HCOO^- dehydrogenation ($E_{\text{barr}} = 1.24 \text{ eV}$) and HCO_3^- hydrogenation ($E_{\text{barr}} = 1.49 \text{ eV}$) were confirmed to be the desorption of hydrogen protons from the Pd NC. The doping of an appropriate dose of pyridine nitrogen could significantly reduce the energy barrier of the reversible reaction by regulating the electronic and geometric effects of the Pd NC (Figure 7), thus improving the efficiency of reversible transformation between HCO_3^- and HCO_2^- .

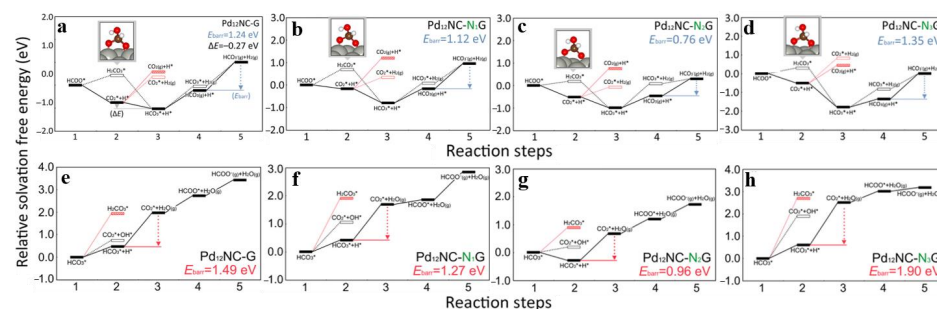


Figure 7. Relative solvation-free energy diagram of (a–d) HCOO^- dehydrogenation and (e–h) HCO_3^- hydrogenation over Pd-based catalyst with different pyridine nitrogen doping amounts. * means adsorptive state. Reproduced with permission from Ref. [92]. Copyright 2018, American Chemical Society.

2.1.4. Mesoporous Graphitic Carbon Nitride-Supported Monometallic Catalysts

In 2014, Yoon et al. reported mesoporous graphitic carbon nitride (mpg-C₃N₄)-immobilized Pd nanoparticles (NPs) for the interconversion between FA and CO₂, which was one of the earliest heterogeneous catalysts for a CO₂-mediated H₂ cycle system [93]. The resulting Pd/mpg-C₃N₄ demonstrated activity for H₂ generation from FA without any base/additive, with a turnover frequency (TOF) of 144 h^{−1} at 25 °C and a TOF of 4 h^{−1} for CO₂ hydrogenation with triethylamine (NEt₃) as the CO₂ absorbent at 150 °C. X-ray absorption near-edge structure (XANES) analysis and DFT calculation revealed that the abundant nitrogen functionalities in the mpg-C₃N₄ support had a pivotal role in stabilizing Pd NPs and activating FA and CO₂, which explained the activity for the reversible H₂ storage-release process. However, the efficiency of CO₂ hydrogenation was rather low in this preliminary study.

In consideration of the vital role of N-doping in the reversible H₂ storage system, Huang, Wang, et al. also prepared mesoporous graphitic carbon nitride (mpg-C₃N₄) by pyrolysis of dicyandiamide to support Pd NPs [94]. The resulting Pd/mpg-C₃N₄ catalyst was proved to be an excellent catalyst for high-concentration KHCO₃ hydrogenation (TOF = 4076 h^{−1}) and the dehydrogenation of HCOOK (511 h^{−1}) at 80 °C. Nitrogen species doped in mpg-C₃N₄ stabilized the Pd NPs with high dispersion and small size, changed the electronic state of the Pd through donating electrons toward the Pd, and formed hydrogen bonds with OH[−] in HCO₃[−], which synergistically boosted the hydrogenation of KHCO₃. In addition, Pd/mpg-C₃N₄ was sturdy and could be reused six times during the hydrogenation reaction and three times during the dehydrogenation reaction. They also provided a possible mechanism for HCO₃[−] hydrogenation catalyzed by Pd/mpg-C₃N₄ (Figure 8). First, HCO₃[−] was adsorbed on the Pd/mpg-C₃N₄ surface through hydrogen bonds between the OH[−] in HCO₃[−] and the N functionalities in mpg-C₃N₄. Then, the positively polarized C in the HCO₃[−] was attacked by the H proton generated by H₂ dissociation on the Pd NPs, forming HCOO[−].

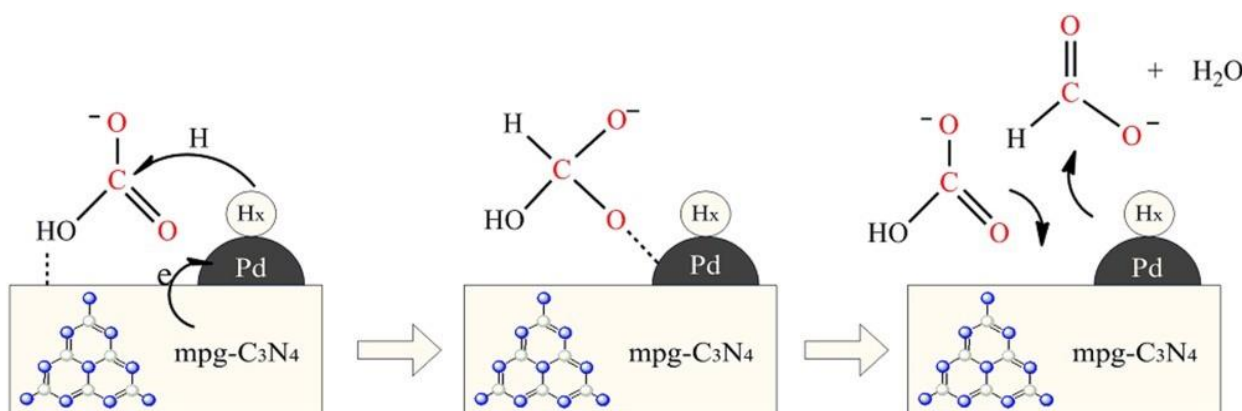


Figure 8. Possible reaction processes of bicarbonate hydrogenation on Pd/mpg-C₃N₄. Reprinted with permission from Ref. [94]. Copyright 2016, Wiley.

The catalytic performance of monometal-based heterogeneous catalysts for the FA-based hydrogen cycle system are summarized in Table 1.

Table 1. Catalytic performance of the monometal-based heterogeneous catalysts for the interconversion between CO₂ (bicarbonate) hydrogenation and FA (formate) dehydrogenation.

Hydrogenation Reaction						Dehydrogenation Reaction				
Catalyst	Substrate	Additive	PH ₂ /PCO ₂ (MPa)	T (°C)	TOF (h ^{−1})	Substrate	Additive	T (°C)	TOF (h ^{−1})	Ref.
Pd/AC	1 M NH ₄ HCO ₃	/	2.75/0	20	118	1 M HCO ₂ NH ₄	/	80	1132	[85]

Table 1. Cont.

Hydrogenation Reaction						Dehydrogenation Reaction				
Catalyst	Substrate	Additive	P _{H₂} /P _{CO₂} (MPa)	T (°C)	TOF (h ^{−1})	Substrate	Additive	T (°C)	TOF (h ^{−1})	Ref.
Pd/AC	CO ₂ ^a	1 M piperidine	2.76/0	30	5945	1 M FPA ^b	/			[86]
Pd/CN _{0.25}	CO ₂	5.7 M NEt ₃	3/3	100	1837	1 M HCOOH	/	25	5530	[87]
Pd/NMC	4 M KHCO ₃	/	6/0	80	799	2 M HCOOK	/	60	1118	[88]
Pd/PDMC	1 M NaHCO ₃	/	4/0	80	68	1 M NaHCO ₂	/	80	2562	[89]
Pd/N,P-C	4 M KHCO ₃	/	8/0	80	2805	4 M KHCO ₂	/	80	3248	[90]
Pd/r-GO	4.8 M KHCO ₃	/	4/0	100	242	4.8 M HCOOK	/	80	11,299	[91]
Pd/mpg-C ₃ N ₄	CO ₂	1.4 M NEt ₃	2/2	150	4	1 M HCOOH	/	25	144	[93]
Pd/mpg-C ₃ N ₄	4 M KHCO ₃	/	8/0	80	4076	4 M HCOOK	/	80	511	[94]

^a Piperidine-captured CO₂. ^b Formate piperidine adducts.

2.2. Bimetal-Based Heterogeneous Catalytic System

2.2.1. Molecular Sieve-Supported Bimetallic Catalysts

In 2017, Yamashita et al. immobilized bimetallic PdAg NPs in the mesoporous silica SBA-15, which was the first study on the potential of bimetallic nanocatalysts in the reversible conversion between FA and CO₂ [95]. To improve the interaction between the metal precursor and support, phenylamine, with a weak basicity functional group, was introduced into the SBA-15 to produce SBA-15-phenylamine support. TEM images showed that the size of the PdAg NPs anchored by the SBA-15-phenylamine was 3.9 nm, which was smaller than that of PdAg/SBA-15 (~10 nm), confirming the reduction in the metal NP size after the introduction of phenylamine. The PdAg/SBA-15-phenylamine catalyst (the molar ratio of the Pd to Ag was 1:1) exhibited activity for H₂ production from FA offering a TOF of 822 h^{−1} (75 °C), with the aid of sodium formate (HCOONa), and a TOF of 36 h^{−1} (100 °C) for CO₂ hydrogenation with NaHCO₃ as the additive. Compared to the corresponding monometallic Pd catalyst, the activity of the PdAg/SBA-15-phenylamine was at least four-fold higher for FA dehydrogenation and at least three-fold higher for CO₂ hydrogenation. However, the corresponding monometallic Ag was inactive in both reactions, suggesting that the Pd was the active site and the Ag only served as a co-catalyst to boost the activity of the Pd. They concluded that the improved activity of the PdAg/SBA-15-phenylamine was primarily due to the generation of smaller PdAg NPs via introducing phenylamine and the synergistic effect between bimetallic components. However, the recycling stability of the PdAg/SBA-15-phenylamine was not satisfactory, and the activity of the FA dehydrogenation and CO₂ hydrogenation was significantly reduced after three recycles.

2.2.2. Zeolite-Supported Bimetallic Catalysts

In 2020, Yan, Yu, et al. confined Pd-Mn bimetallic clusters to silicalite-1 zeolites via a ligand-protected approach (Figure 9a) [96]. The aberration-corrected STEM-HAADF images showed that the size of the monometallic Pd and PdMn clusters was similar, about 1 nm or smaller, indicating that the introduction of Mn components did not change the size of the Pd clusters (Figure 9b–e). XPS measurement confirmed that most Pd and Mn species in the PdMnx@S-1 sample were confined within the zeolite crystals. The results of thermal stability investigation demonstrated that PdMn_{0.6}@S-1 displayed significantly enhanced the

thermal stability compared to Pd/S-1-im synthesized via an incipient wetness impregnation approach. XANES and in situ analysis revealed that the introduction of Mn components facilitated the formation of electron-rich Pd in PdMn_{0.6}@S-1 through electron transfer from the Mn to the Pd. The resultant PdMn_{0.6}@S-1 catalyst achieved a TOF of 2151 h⁻¹ for formate generation by CO₂ hydrogenation at 80 °C and an initial TOF of 6860 h⁻¹ for CO-free H₂ release by FA decomposition at 60 °C. The observed high activity of the CO₂ hydrogenation and FA decomposition gave credit to the generation of highly dispersed metal clusters and a synergistic effect of the bimetallic components in the PdMn_{0.6}@S-1. Moreover, PdMn_{0.6}@S-1 also displayed excellent reusability in the CO₂ hydrogenation and FA decomposition reactions, with an unchanged formate generation rate and H₂ release rate after five consecutive runs, respectively.

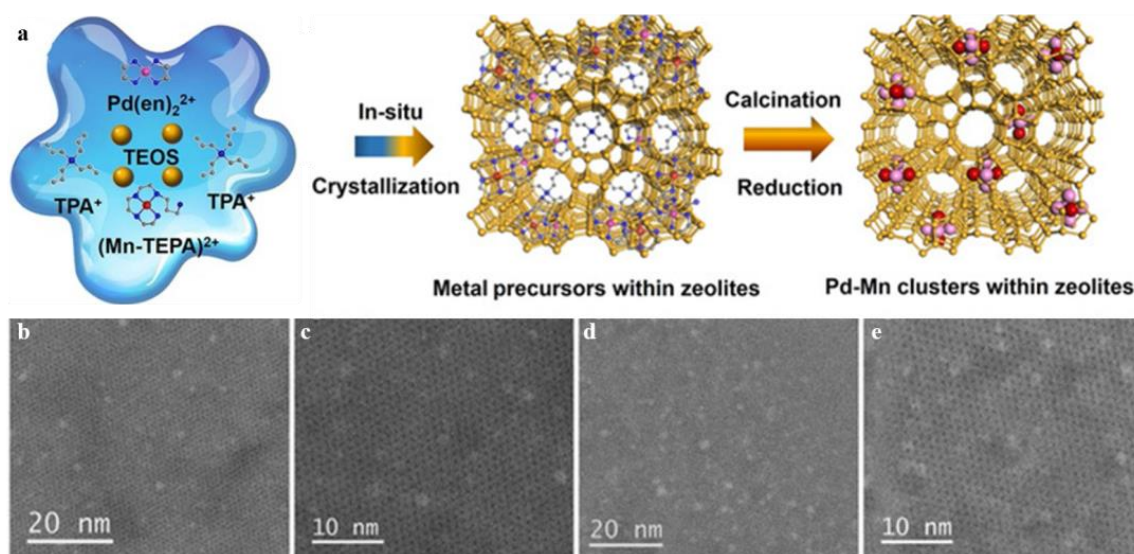


Figure 9. (a) Synthetic schematic of PdMnx@S-1. STEM-HAADF images of (b,c) Pd@S-1 and (d,e) PdMn_{0.6}@S-1. Reproduced with permission from Ref. [96]. Copyright 2020, Wiley.

2.2.3. Activated Carbon-Supported Bimetallic Catalysts

In 2019, Shishido et al. revealed the correlation between the electronic property and structure of bimetallic alloys and the activity for reversible conversion between NH₄HCO₃ and NH₄HCO₂ through activated carbon-supported Pd-Au alloy catalysts (AuPd/AC) [97]. HAADF-STEM characterization indicated that the mean size of AuPd NPs in the AuPd/AC with a Au/Pd molar ratio of 0.1~10 was ca. 3 nm. XPS and XAFS analyses both proved the transfer of electrons from the Pd to the Au in the bimetallic catalyst. According to the coordination number derived from EXAFS characterization, the configuration and distribution of the Au and Pd atoms on the bimetallic alloy NP surface changed with the Au/Pd molar composition (Figure 10a). If the ratio of the Au/Pd was high, Au atoms encircled a single Pd atom (10Au1Pd/AC). If the molar ratio of the Au/Pd was 1 (1Au1Pd/AC), the Pd atoms were encircled by equal amounts of Pd and Au atoms. The reaction results demonstrated that all the Pd-Au/AC binary catalysts demonstrated superior activity than that of the corresponding monometallic species for reversible hydrogenation and dehydrogenation reactions. The difference in the electronic state and local structure of AuPd bimetallic NPs caused by different bimetallic compositions affected their catalytic activity for the reversible reaction. For the hydrogenation of NH₄HCO₃ (Figure 10b), the TOF value increased monotonically with an increasing Au/Pd molar ratio, and 10Au1Pd/AC exhibited the best activity, with a TOF of 5820 h⁻¹ at 60 °C. Whereas a volcano-type relationship was found between the TOF values for H₂ production and the Au/Pd ratios (Figure 10c), the optimum catalyst was 1Au1Pd/AC, exhibiting the best TOF of 4200 h⁻¹ at 40 °C.

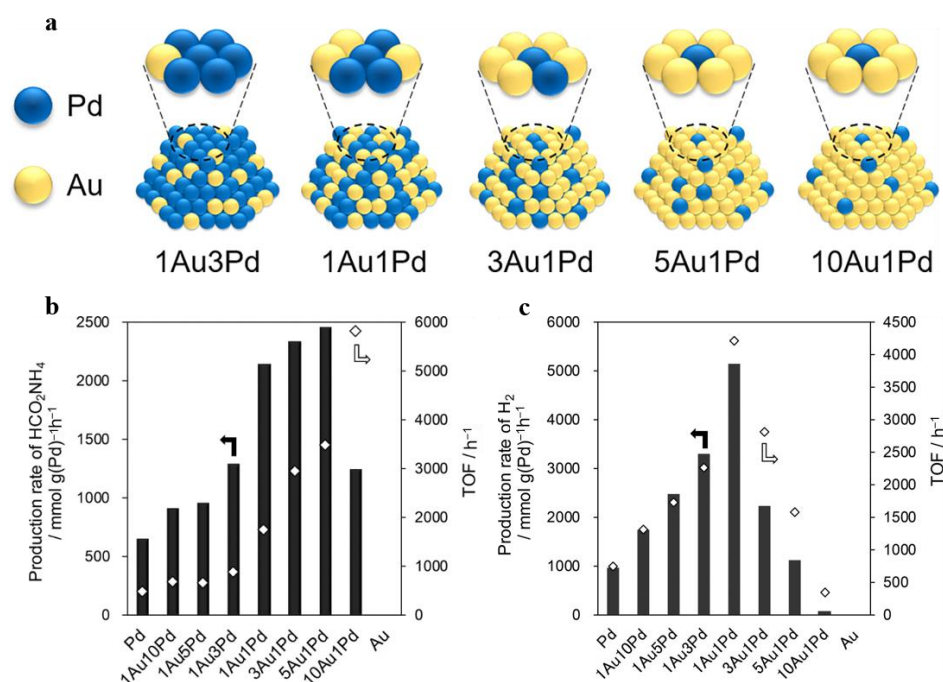


Figure 10. (a) Pd-Au bimetallic NP structures with different molar compositions. (b) Production rate of NH_4HCO_2 and corresponding TOF values over different catalysts. Conditions: 0.1 g catalyst, 20 mL 1 M NH_4HCO_3 , 5 MPa H_2 , and 60 °C. (c) H_2 generation rate and corresponding TOF values over different catalysts. Reaction conditions: 0.1 g catalyst, 4 mL 1 M NH_4HCO_2 , and 40 °C. Reprinted with permission from Ref. [97]. Copyright 2019, American Chemical Society.

Liang, Huang, et al. synthesized Pd-Au/AC and Pd-Cu/AC bimetallic catalysts using a biomass-reduction method and investigated their catalytic activities for the interconversion between CO_2 and FA [98]. Monometallic Cu/AC and Au/AC demonstrated negligible activity for CO_2 hydrogenation to formate. The TOF values at 110 °C of the Pd-Au/AC (81 h $^{-1}$) and Pd-Cu/AC (100 h $^{-1}$) for formate generation were 1.9 and 2.4 times that of the Pd/AC (43 h $^{-1}$), respectively. In addition, the activity of the bimetallic catalysts was remarkably superior to that of the corresponding mixture of monometallic catalysts, indicating the existence of synergistic effects between the Pd and doped metals. Concomitantly, the synergistic effect between the metal components made both the Pd-Cu/AC and Pd-Au/AC bimetallic catalysts exhibit FA dehydrogenation activity with a TOF of 101 h $^{-1}$ and 431 h $^{-1}$ at 80 °C, respectively. As shown in Table 2, the downshift of Pd 3d binding energies in the bimetallic catalysts indicated that the electron donor capability of Au and Cu toward the Pd affected the electron property of the Pd, thus improving the hydrogenation and dehydrogenation activity of the Pd-based bimetallic catalyst.

Table 2. Comparison of Pd 0 binding energies in different Pd-based catalysts. Reproduced with permission from Ref. [98]. Copyright 2022, American Chemical Society.

Catalyst Sample	Binding Energy (eV)	
	Pd 0 3d $_{3/2}$	Pd 0 3d $_{5/2}$
Pd/AC	341.28	335.92
Pd-Cu/AC	341.18	335.86
Pd-Au/AC	341.06	335.73

Very recently, Ren et al. synthesized L-arginine-modified carbon-anchored PdAu alloy catalysts (PdAu/AC-LA) for reversible H_2 storage under ambient conditions [99]. By adjusting the introduction amount of LA and the composition of Pd and Au, the optimal catalyst Pd $_1$ Au $_2$ /AC-LA showed good activity for H_2 release from FA (TOFs = 1760 h $^{-1}$)

and CO₂ hydrogenation (TOFs = 138 h^{−1}) at 25 °C. The comprehensive characterization results demonstrated that the alloying effect of the PdAu and the modification of the strongly basic L-arginine improved the adsorption of the reactants (Figure 11), thus increasing the activity of the Pd₁Au₂/AC-LA.

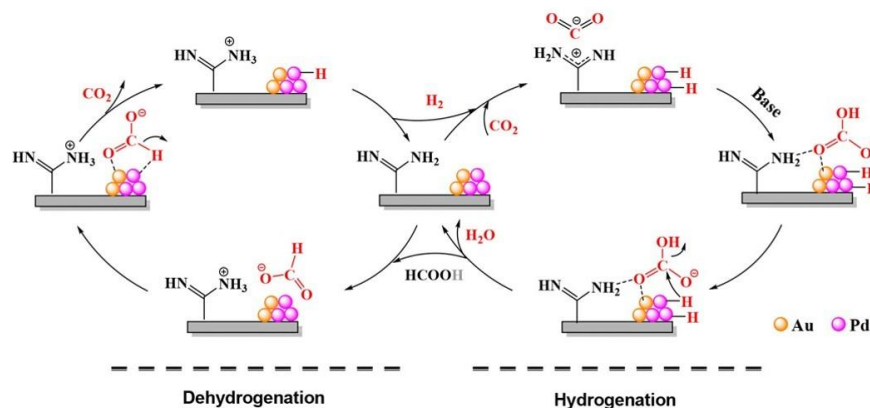


Figure 11. Plausible reaction process of CO₂ hydrogenation and FA dehydrogenation on Pd₁Au₂/AC-LA. Reprinted with permission from Ref. [99]. Copyright 2022, American Chemical Society.

2.2.4. Mesoporous Carbon-Supported Bimetallic Catalysts

To develop more powerful catalysts for the reversible conversion between FA and CO₂, the same research group modified the mesoporous carbon with p-phenylenediamine (amine-MSC) to load PdAg NPs in 2018 [100]. TEM measurements revealed that the average NP diameters of PdAg/amine-MSC and PdAg/MSC were 1.2 and 2.3 nm, respectively. Compared with the support of SBA-15, the MSC appeared to be more conducive to controlling the dispersion and size of the active metals. In addition, amine groups in the MSC could further reduce the size of metal NPs through the interaction of the metal precursor and the support. The reaction results showed that the TOF values for FA dehydrogenation and CO₂ hydrogenation were 5638 h^{−1} (75 °C) and 35 h^{−1} (100 °C), respectively. Experimental explorations and DFT calculation showed that functional groups in phenylamine played a crucial role in not only the determination of the metal NP size but also the adsorption and activation of the FA and CO₂ in the catalytic cycle (Figure 12). Additionally, PdAg/amine-MSC can be reused for at least three cycles for the reversible conversion between FA and CO₂ without any decline in its catalytic activity, exhibiting good reversibility and recyclability.

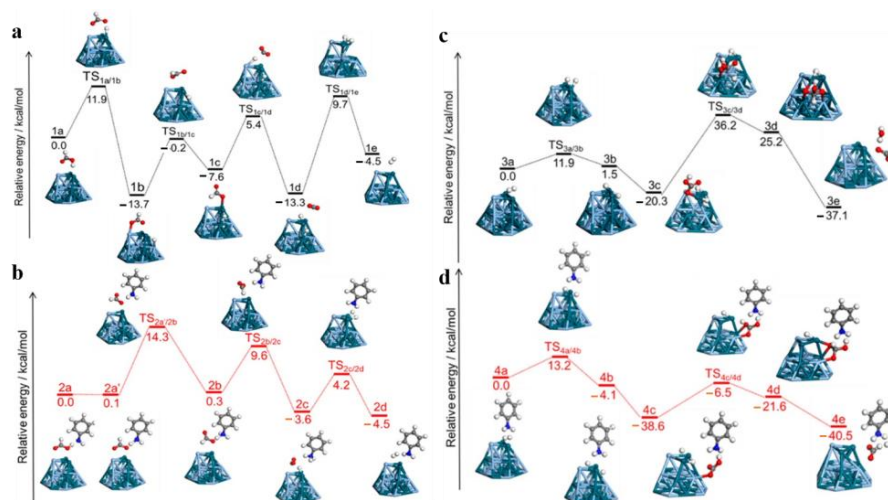


Figure 12. Potential energy profiles for H₂ generation from FA (a) without and (b) with phenylamine. Potential energy profiles for CO₂ hydrogenation (c) without and (d) with phenylamine. Reproduced with permission from Ref. [100]. Copyright 2020, American Chemical Society.

2.2.5. Graphene-Supported Bimetallic Catalysts

In the same year, Kawanami et al. grafted p-phenylenediamine (PDA) into reduced graphene oxide to form a PDA-rGO support [101]. Bimetallic PdAu NPs with various Pd/Au molar compositions were anchored in the PDA-rGO support through an impregnation method coupled with NaBH_4 reduction. The average size of the PdAu NPs in all the bimetallic PdAu/PDA-rGO was about 1.8 nm. The resulting PdAu/PDA-rGO catalysts were employed for KHCO_3 hydrogenation and the dehydrogenation of HCOOK and FA. The catalytic activity of all the PdAu bimetallic catalysts was superior to that of corresponding monometallic catalysts for the reversible H_2 storage system. The composition of PdAu bimetallic NPs dramatically affected the activity of the PdAu/PDA-rGO catalysts. Among them, the $\text{Pd}_{0.5}\text{Au}_{0.5}$ /PDA-rGO catalyst with a molar composition of Pd/Au of 1/1 demonstrated the highest catalytic activity. For KHCO_3 hydrogenation, a 94% HCOOK yield was achieved at 50 °C. The $\text{TOF}_{\text{initial}}$ values for high-concentration HCOOK (6 M) and FA (8 M) dehydrogenation reached 1630 h^{-1} and 6980 h^{-1} at 80 °C, respectively. The authors suggested that the stabilizing effect of the PDA on the metal NPs and the electronic regulation of the Pd by Au synergistically promoted the catalytic activity of the $\text{Pd}_{0.5}\text{Au}_{0.5}$ /PDA-rGO. However, the influence of the local structure and electronic state of PdAu alloys with different compositions on the activity of catalysts has not been studied in depth. In addition, the catalyst was not stable due to the conversion and leaching of the PDA during the reaction under high-pressure conditions (3–7 MPa of H_2).

2.2.6. Metal Oxide-Supported Bimetallic Catalysts

In 2020, Mori, Yamashita, et al. explored the effect of a Pd-Ag alloy structure on the interconversion between HCOONa and NaHCO_3 , including a PdAg solid solution (PdAg), a Pd core-Ag shell structure (Pd@Ag), and a Ag core-Pd shell structure (Ag@Pd) [102]. As shown in Figure 13a, the alloy structure greatly affected the electronic property and activity of the Pd for reversible reactions. Among various alloy structures, Pd@Ag/ TiO_2 with electron-rich Pd demonstrated the highest activity for HCOONa dehydrogenation and NaHCO_3 hydrogenation with TOF values (calculated based on the surface Pd atoms) of 20,578 and 1568 h^{-1} , respectively. To further improve the catalytic activity, the authors modified these alloy catalysts with TiO_x shells. As shown in Figure 13b, the introduction of TiO_x shells facilitated the improvement of the activity of all the Pd-Ag alloy catalysts. They concluded that the generation of the Pd- TiO_2 interface was responsible for the improved catalytic activity. The characterization results and kinetic studies revealed that the generation of the Pd-Ag alloy and Pd- TiO_2 interface facilitated the cleavage of the C–H bonds in HCOONa dehydrogenation and improved the adsorption and activation of bicarbonate during the hydrogenation process.

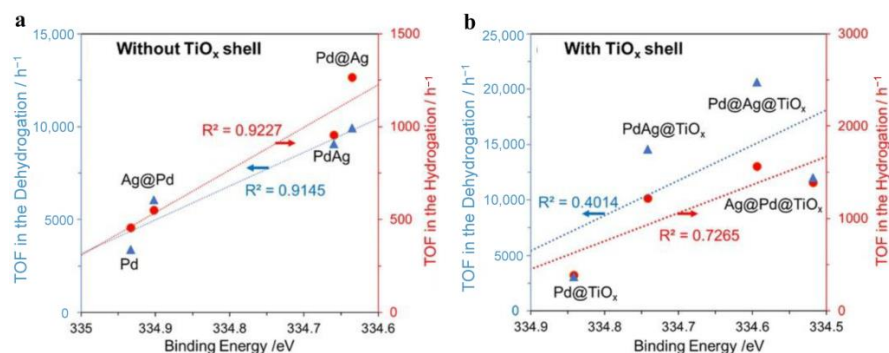


Figure 13. Correlation between Pd 3d binding energy and catalytic activities for HCOONa dehydrogenation and NaHCO_3 hydrogenation (a) without and (b) with TiO_x shells. Dehydrogenation reaction conditions: 50 mg catalyst, 10 mL 1 M HCOONa aqueous solution, and 75 °C. Hydrogenation reaction conditions: 20 mg catalyst, 15 mL 1 M NaHCO_3 aqueous solution, 80 °C, and 3.0 MPa H_2 . Reprinted with permission from Ref. [102]. Copyright 2020, American Chemical Society.

The catalytic performance of bimetal-based heterogeneous catalysts for an FA-based hydrogen cycle system are summarized in Table 3.

Table 3. Catalytic performance of the bimetal-based heterogeneous catalysts for the interconversion between CO₂ (bicarbonate) hydrogenation and FA (formate) dehydrogenation.

Hydrogenation Reaction						Dehydrogenation Reaction				Ref.
Catalyst	Substrate	Additive	P _{H₂} /P _{CO₂} (MPa)	T (°C)	TOF (h ^{−1})	Substrate	Additive	T (°C)	TOF (h ^{−1})	
PdAg/SBA-15-phenylamine	CO ₂	1 M NaHCO ₃	1/1	100	36	0.9 M HCCOH	0.1 M HCOONa	75	822	[95]
PdMn _{0.6} @S-1	CO ₂	1.5 M NaOH	2/2	80	2151	2 M HCOOH	/	60	6860	[96]
10Au1Pd/AC	1 M NH ₄ HCO ₃	/	5/0	60	5820	1 M HCO ₂ NH ₄	/	40	4200	[97]
Pd-Au/AC	CO ₂	1.8 M NEt ₃	5/5	110	81	1 M HCOOH	0.5 M NEt ₃	80	431	[98]
Pd-Cu/AC	CO ₂	1.8 M NEt ₃	3.5/3.5	110	100	1 M HCOOH	0.5 M NEt ₃	80	101	
Pd ₁ Au ₂ /AC-LA	CO ₂	1 M NaHCO ₃	0.075/0.025	25	138	1 M HCOOH	/	25	1760	[99]
PdAg/amine-MSC	CO ₂	1 M NaHCO ₃	1/1	100	35	0.27 M HCOOH	0.03 M HCOONa	75	5638	[100]
Pd _{0.50} Au _{0.50} /PDA-rGO	0.5 M KHCO ₃	/	5/0	50	/	6 M HCOOK	/	80	1630	[101]
						8 M HCOOH	/	80	6980	
Pd@Ag/TiO ₂	NaHCO ₃	/	3/0	80	1568	HCOONa	/	75	20,578	[102]

3. Conclusions and Perspectives

In summary, many strategies have been devoted to improving the activation of heterogeneous catalysts for FA-based hydrogen cycle systems, chiefly in the construction of electron-rich Pd-based catalysts through the introduction of electron-donating ligands. For example, the doping of N and/or P elements, the grafting of organic functional groups, and the formation of bimetallic alloys are believed to provide stability and induce geometrical and electronic effects of active metal, which determine the final catalytic performance. Although many efforts have been made in this field, there are still significant challenges that motivate researchers to develop efficient catalysts to construct a practical FA-based hydrogen cycle system.

Firstly, although the reported heterogeneous catalysts showed superior activity and selectivity for the dehydrogenation of FA (formate) under mild conditions, the efficiency for CO₂ (bicarbonate) hydrogenation was still far from satisfactory due to the strong thermodynamic stability and kinetic inertness of CO₂ molecules. Furthermore, the reaction of CO₂ hydrogenation is generally proceeded under high-temperature and high-pressure conditions and requires alkaline additives. Therefore, developing highly efficient CO₂ hydrogenation catalysts under mild conditions remains a challenge for a carbon-neutral hydrogen cycle system.

Secondly, amine-functionalized or N-doped support materials are usually prepared to enhance the activity of Pd-based catalysts for the reversible reaction between CO₂ (bicarbonate) and FA (formate). The nitrogen-containing groups in these materials are usually monodentate ligands, while support materials modified with polydentate and pincer-type ligands have rarely been studied, which are commonly used in homogeneous catalysis systems.

Thirdly, to date, the heterogeneous catalysts commonly used in the FA-based hydrogen storage and release system are Pd-based catalysts, and it still needs to develop other efficient and stable transition metal catalysts or non-noble metal catalysts.

With this comprehensive overview, it is believed that the readers could understand the current trends in designing and evaluating heterogeneous catalysts for efficient H₂

storage-release systems. We hope this review can shed light on the design and development of efficient heterogeneous catalysts for a carbon-neutral hydrogen cycle system.

Author Contributions: Z.W.: provided ideas, conducted the extensive literature investigation, and wrote the original draft. Z.S. and Z.Z. participated in the discussion and revised the paper. J.Q., M.H., and Q.C. participated in the discussion and supervised the project. All authors have read and agreed to the published version of the manuscript.

Funding: This research was funded by the Jiangsu Key Laboratory of Advanced Catalytic Materials and Technology, grant number BM2012110.

Data Availability Statement: Not available.

Conflicts of Interest: The authors declare no conflict of interest.

References

- Kar, S.; Rauch, M.; Leitus, G.; Ben-David, Y.; Milstein, D. Highly efficient additive-free dehydrogenation of neat formic acid. *Nat. Catal.* **2021**, *4*, 193–201. [\[CrossRef\]](#)
- Eppinger, J.; Huang, K.W. Formic Acid as a Hydrogen Energy Carrier. *ACS Energy Lett.* **2016**, *2*, 188–195. [\[CrossRef\]](#)
- Chen, H.; Shuang, H.; Lin, W.; Li, X.; Zhang, Z.; Li, J.; Fu, J. Tuning Interfacial Electronic Properties of Palladium Oxide on Vacancy-Abundant Carbon Nitride for Low-Temperature Dehydrogenation. *ACS Catal.* **2021**, *11*, 6193–6199. [\[CrossRef\]](#)
- Wei, D.; Sang, R.; Sponholz, P.; Junge, H.; Beller, M. Reversible hydrogenation of carbon dioxide to formic acid using a Mn-pincer complex in the presence of lysine. *Nat. Energy* **2022**, *7*, 438–447. [\[CrossRef\]](#)
- Park, K.; Gunasekar, G.H.; Kim, S.H.; Park, H.; Kim, S.; Park, K.; Jung, K.D.; Yoon, S. CO₂ hydrogenation to formic acid over heterogenized ruthenium catalysts using a fixed bed reactor with separation units. *Green Chem.* **2020**, *22*, 1639–1649. [\[CrossRef\]](#)
- Onishi, N.; Iguchi, M.; Yang, X.; Kanega, R.; Kawanami, H.; Xu, Q.; Himeda, Y. Development of Effective Catalysts for Hydrogen Storage Technology Using Formic Acid. *Adv. Energy Mater.* **2018**, *9*, 1801275. [\[CrossRef\]](#)
- Amos, R.I.J.; Heinroth, F.; Chan, B.; Ward, A.J.; Zheng, S.; Haynes, B.S.; Easton, C.J.; Masters, A.F.; Maschmeyer, T.; Radom, L. Hydrogen from Formic Acid via Its Selective Disproportionation over Nanodomain-Modified Zeolites. *ACS Catal.* **2015**, *5*, 4353–4362. [\[CrossRef\]](#)
- Zhang, Z.; Liu, S.; Hou, M.; Yang, G.; Han, B. Continuous-flow formic acid production from the hydrogenation of CO₂ without any base. *Green Chem.* **2021**, *23*, 1978–1982. [\[CrossRef\]](#)
- Graetz, J. New approaches to hydrogen storage. *Chem. Soc. Rev.* **2009**, *38*, 73–82. [\[CrossRef\]](#)
- Murray, L.J.; Dinca, M.; Long, J.R. Hydrogen storage in metal-organic frameworks. *Chem. Soc. Rev.* **2009**, *38*, 1294–1314. [\[CrossRef\]](#)
- Sousa-Castillo, A.; Li, F.; Carbo-Argibay, E.; Correa-Duarte, M.A.; Klinkova, A. Pd-CNT-SiO₂ nanoskein: Composite structure design for formic acid dehydrogenation. *Chem. Commun.* **2019**, *55*, 10733–10736. [\[CrossRef\]](#)
- Liu, H.; Lei, Q.; Miao, R.; Sun, M.; Qin, C.; Zhang, L.; Ye, G.; Yao, Y.; Huang, B.; Ma, Z. Asymmetric Coordination of Single-Atom Co Sites Achieves Efficient Dehydrogenation Catalysis. *Adv. Funct. Mater.* **2022**, *32*, 220408. [\[CrossRef\]](#)
- Wang, Z.; Liang, S.; Meng, X.; Mao, S.; Lian, X.; Wang, Y. Ultrasmall PdAu alloy nanoparticles anchored on amine-functionalized hierarchically porous carbon as additive-free catalysts for highly efficient dehydrogenation of formic acid. *Appl. Catal. B* **2021**, *291*, 120140. [\[CrossRef\]](#)
- Wang, Z.; Wang, C.; Mao, S.; Gong, Y.; Chen, Y.; Wang, Y. Pd nanoparticles anchored on amino-functionalized hierarchically porous carbon for efficient dehydrogenation of formic acid under ambient conditions. *J. Mater. Chem. A* **2019**, *7*, 25791–25795. [\[CrossRef\]](#)
- Yan, J.M.; Li, S.J.; Yi, S.S.; Wulan, B.R.; Zheng, W.T.; Jiang, Q. Anchoring and Upgrading Ultrafine NiPd on Room-Temperature-Synthesized Bifunctional NH₂-N-rGO toward Low-Cost and Highly Efficient Catalysts for Selective Formic Acid Dehydrogenation. *Adv. Mater.* **2018**, *30*, 1703038. [\[CrossRef\]](#)
- Li, D.; Li, Y.; Liu, X.; Guo, Y.; Pao, C.W.; Chen, J.L.; Hu, Y.; Wang, Y. NiAl₂O₄ Spinel Supported Pt Catalyst: High Performance and Origin in Aqueous-Phase Reforming of Methanol. *ACS Catal.* **2019**, *9*, 9671–9682. [\[CrossRef\]](#)
- Chen, L.N.; Hou, K.P.; Liu, Y.S.; Qi, Z.Y.; Zheng, Q.; Lu, Y.H.; Chen, J.Y.; Chen, J.L.; Pao, C.W.; Wang, S.B.; et al. Efficient Hydrogen Production from Methanol Using a Single-Site Pt₁/CeO₂ Catalyst. *J. Am. Chem. Soc.* **2019**, *141*, 17995–17999. [\[CrossRef\]](#)
- Lin, L.; Zhou, W.; Gao, R.; Yao, S.; Zhang, X.; Xu, W.; Zheng, S.; Jiang, Z.; Yu, Q.; Li, Y.W.; et al. Low-temperature hydrogen production from water and methanol using Pt/ α -MoC catalysts. *Nature* **2017**, *544*, 80–83. [\[CrossRef\]](#)
- Meng, Y.; Sun, Q.; Zhang, T.; Zhang, J.; Dong, Z.; Ma, Y.; Wu, Z.; Wang, H.; Bao, X.; Sun, Q.; et al. Cobalt-Promoted Noble-Metal Catalysts for Efficient Hydrogen Generation from Ammonia Borane Hydrolysis. *J. Am. Chem. Soc.* **2023**, *145*, 5486–5495. [\[CrossRef\]](#)
- Zhang, J.; Yu, W.; Feng, D.; Xu, H.; Qin, Y. Porous titania nanotube confined ultrafine platinum catalysts synthesized by atomic layer deposition with enhanced hydrolytic dehydrogenation performance. *Appl. Catal. B* **2022**, *312*, 121405. [\[CrossRef\]](#)
- Guan, S.; Liu, Y.; Zhang, H.; Wei, H.; Liu, T.; Wu, X.; Wen, H.; Shen, R.; Mehdi, S.; Ge, X.; et al. Atomic Interface-Exciting Catalysis on Cobalt Nitride-Oxide for Accelerating Hydrogen Generation. *Small* **2022**, *18*, e2107417. [\[CrossRef\]](#) [\[PubMed\]](#)

22. Li, X.; Yao, Q.; Shi, R.; Huang, M.; Lu, Z.H. A step-growth strategy to grow vertical porous aromatic framework nanosheets on graphene oxide: Hybrid material-confined Co for ammonia borane methanolysis. *Carbon Energy* **2023**, e3572023.
23. Xu, F.; Wang, Y.; Wang, C.; Huang, W.; Liu, X. Dehydrogenation of hydrous hydrazine over carbon nanosphere-supported PtNi nanoparticles for on-demand H₂ release. *Fuel* **2023**, 332, 126116. [\[CrossRef\]](#)
24. Wang, C.; Astruc, D. Recent developments of nanocatalyzed liquid-phase hydrogen generation. *Chem. Soc. Rev.* **2021**, 50, 3437–3484. [\[PubMed\]](#)
25. Luo, F.; Miao, X.; Chu, W.; Wu, P.; Tong, D.G. Retracted Article: Preparation of face-centered-cubic indium nanocubes and their superior dehydrogenation activity towards aqueous hydrazine with the assistance of light. *J. Mater. Chem. A* **2016**, 4, 17665–17672.
26. Zhang, Y.; Lyu, Y.; Wang, Y.; Li, C.; Jiang, M.; Ding, Y. Highly active and stable porous polymer heterogeneous catalysts for decomposition of formic acid to produce H₂. *Chin. J. Catal.* **2019**, 40, 147–151. [\[CrossRef\]](#)
27. Qin, X.; Li, H.; Xie, S.; Li, K.; Jiang, T.; Ma, X.Y.; Jiang, K.; Zhang, Q.; Terasaki, O.; Wu, Z.; et al. Mechanistic Analysis-Guided Pd-Based Catalysts for Efficient Hydrogen Production from Formic Acid Dehydrogenation. *ACS Catal.* **2020**, 10, 3921–3932. [\[CrossRef\]](#)
28. Yang, X.; Xu, Q. Gold-containing metal nanoparticles for catalytic hydrogen generation from liquid chemical hydrides. *Chin. J. Catal.* **2016**, 37, 1594–1599.
29. Hou, T.; Luo, Q.; Li, Q.; Zu, H.; Cui, P.; Chen, S.; Lin, Y.; Chen, J.; Zheng, X.; Zhu, W.; et al. Modulating oxygen coverage of Ti₃C₂T_x MXenes to boost catalytic activity for HCOOH dehydrogenation. *Nat. Commun.* **2020**, 11, 4251. [\[CrossRef\]](#)
30. Shao, X.; Yang, X.; Xu, J.; Liu, S.; Miao, S.; Liu, X.; Su, X.; Duan, H.; Huang, Y.; Zhang, T. Iridium Single-Atom Catalyst Performing a Quasi-homogeneous Hydrogenation Transformation of CO₂ to Formate. *Chem* **2019**, 5, 693–705. [\[CrossRef\]](#)
31. Akbayrak, S.; Tonbul, Y.; Özkar, S. Nanoceria supported palladium(0) nanoparticles: Superb catalyst in dehydrogenation of formic acid at room temperature. *Appl. Catal. B* **2017**, 206, 384–392. [\[CrossRef\]](#)
32. Zhang, Q.; Zhu, Z.; Zhang, X.; Li, P.; Huang, Y.; Luo, X.; Liang, Z. Amine-functionalized sepiolite: Toward highly efficient palladium nanocatalyst for dehydrogenation of additive-free formic acid. *Int. J. Hydrogen Energy* **2019**, 44, 16707–16717. [\[CrossRef\]](#)
33. Zhang, S.; Qian, Y.; Ahn, W. Catalytic dehydrogenation of formic acid over palladium nanoparticles immobilized on fibrous mesoporous silica KCC-1. *Chin. J. Catal.* **2019**, 40, 1704–1712. [\[CrossRef\]](#)
34. Yang, Y.; Xu, H.; Cao, D.; Zeng, X.C.; Cheng, D. Hydrogen Production via Efficient Formic Acid Decomposition: Engineering the Surface Structure of Pd-Based Alloy Catalysts by Design. *ACS Catal.* **2018**, 9, 781–790. [\[CrossRef\]](#)
35. Zhai, S.; Jiang, S.; Liu, C.; Li, Z.; Yu, T.; Sun, L.; Ren, G.; Deng, W. Liquid Sunshine: Formic Acid. *J. Phys. Chem. Lett.* **2022**, 13, 8586–8600. [\[CrossRef\]](#)
36. Li, Z.; Yang, X.; Tsumori, N.; Liu, Z.; Himeda, Y.; Autrey, T.; Xu, Q. Tandem Nitrogen Functionalization of Porous Carbon: Toward Immobilizing Highly Active Palladium Nanoclusters for Dehydrogenation of Formic Acid. *ACS Catal.* **2017**, 7, 2720–2724. [\[CrossRef\]](#)
37. Han, L.; Zhang, L.; Wu, H.; Zu, H.; Cui, P.; Guo, J.; Guo, R.; Ye, J.; Zhu, J.; Zheng, X.; et al. Anchoring Pt Single Atoms on Te Nanowires for Plasmon-Enhanced Dehydrogenation of Formic Acid at Room Temperature. *Adv. Sci.* **2019**, 6, 1900006. [\[CrossRef\]](#) [\[PubMed\]](#)
38. Chen, B.; Dong, M.; Liu, S.; Xie, Z.; Yang, J.; Li, S.; Wang, Y.; Du, J.; Liu, H.; Han, B. CO₂ Hydrogenation to Formate Catalyzed by Ru Coordinated with a N,P-Containing Polymer. *ACS Catal.* **2020**, 10, 8557–8566. [\[CrossRef\]](#)
39. Zhang, Z.; Xie, Y.; Li, W.; Hu, S.; Song, J.; Jiang, T.; Han, B. Hydrogenation of carbon dioxide is promoted by a task-specific ionic liquid. *Angew. Chem. Int. Ed.* **2008**, 47, 1127–1129. [\[CrossRef\]](#)
40. Liu, Q.; Yang, X.; Li, L.; Miao, S.; Li, Y.; Li, Y.; Wang, X.; Huang, Y.; Zhang, T. Direct catalytic hydrogenation of CO₂ to formate over a Schiff-base-mediated gold nanocatalyst. *Nat. Commun.* **2017**, 8, 1407. [\[CrossRef\]](#) [\[PubMed\]](#)
41. Wang, Q.; Santos, S.; Urbina-Blanco, C.A.; Hernández, W.Y.; Impérator-Clerc, M.; Vovk, E.I.; Marinova, M.; Ersen, O.; Baaziz, W.; Safonova, O.V.; et al. Solid micellar Ru single-atom catalysts for the water-free hydrogenation of CO₂ to formic acid. *Appl. Catal. B* **2021**, 290, 120036. [\[CrossRef\]](#)
42. Li, Z.; Rayder, T.M.; Luo, L.; Byers, J.A.; Tsung, C.K. Aperture-Opening Encapsulation of a Transition Metal Catalyst in a Metal-Organic Framework for CO₂ Hydrogenation. *J. Am. Chem. Soc.* **2018**, 140, 8082–8085. [\[CrossRef\]](#)
43. Kim, E.H.; Lee, M.H.; Kim, J.; Ra, E.C.; Lee, J.H.; Lee, J.S. Synergy between single atoms and nanoclusters of Pd/g-C₃N₄ catalysts for efficient base-free CO₂ hydrogenation to formic acid. *Chin. J. Catal.* **2023**, 47, 214–221. [\[CrossRef\]](#)
44. Zhou, Z.; Gao, P. Direct carbon dioxide hydrogenation to produce bulk chemicals and liquid fuels via heterogeneous catalysis. *Chin. J. Catal.* **2022**, 43, 2045–2056. [\[CrossRef\]](#)
45. Doustkhah, E.; Hasani, M.; Ide, Y.; Assadi, M.H.N. Pd Nanoalloys for H₂ Generation from Formic Acid. *ACS Appl. Nano Mater.* **2019**, 3, 22–43. [\[CrossRef\]](#)
46. Hong, W.; Kitta, M.; Tsumori, N.; Himeda, Y.; Autrey, T.; Xu, Q. Immobilization of highly active bimetallic PdAu nanoparticles onto nanocarbons for dehydrogenation of formic acid. *J. Mater. Chem. A* **2019**, 7, 18835–18839. [\[CrossRef\]](#)
47. Luo, Y.; Yang, Q.; Nie, W.; Yao, Q.; Zhang, Z.; Lu, Z.H. Anchoring IrPdAu Nanoparticles on NH₂-SBA-15 for Fast Hydrogen Production from Formic Acid at Room Temperature. *ACS Appl. Mater. Interfaces* **2020**, 12, 8082–8090. [\[CrossRef\]](#) [\[PubMed\]](#)
48. Wang, N.; Sun, Q.; Bai, R.; Li, X.; Guo, G.; Yu, J. In Situ Confinement of Ultrasmall Pd Clusters within Nanosized Silicalite-1 Zeolite for Highly Efficient Catalysis of Hydrogen Generation. *J. Am. Chem. Soc.* **2016**, 138, 7484–7487. [\[CrossRef\]](#)

49. Li, S.J.; Zhou, Y.T.; Kang, X.; Liu, D.X.; Gu, L.; Zhang, Q.H.; Yan, J.M.; Jiang, Q. A Simple and Effective Principle for a Rational Design of Heterogeneous Catalysts for Dehydrogenation of Formic Acid. *Adv. Mater.* **2019**, *31*, e1806781. [\[CrossRef\]](#)
50. Moret, S.; Dyson, P.J.; Laurenczy, G. Direct synthesis of formic acid from carbon dioxide by hydrogenation in acidic media. *Nat. Commun.* **2014**, *5*, 4017. [\[CrossRef\]](#)
51. Mori, K.; Sano, T.; Kobayashi, H.; Yamashita, H. Surface Engineering of a Supported PdAg Catalyst for Hydrogenation of CO₂ to Formic Acid: Elucidating the Active Pd Atoms in Alloy Nanoparticles. *J. Am. Chem. Soc.* **2018**, *140*, 8902–8909. [\[CrossRef\]](#)
52. Mellmann, D.; Sponholz, P.; Junge, H.; Beller, M. Formic acid as a hydrogen storage material—Development of homogeneous catalysts for selective hydrogen release. *Chem. Soc. Rev.* **2016**, *45*, 3954–3988. [\[CrossRef\]](#) [\[PubMed\]](#)
53. Hull, J.F.; Himeda, Y.; Wang, W.H.; Hashiguchi, B.; Periana, R.; Szalda, D.J.; Muckerman, J.T.; Fujita, E. Reversible hydrogen storage using CO₂ and a proton-switchable iridium catalyst in aqueous media under mild temperatures and pressures. *Nat. Chem.* **2012**, *4*, 383–388. [\[CrossRef\]](#) [\[PubMed\]](#)
54. Liu, M.; Xu, Y.; Meng, Y.; Wang, L.; Wang, H.; Huang, Y.; Onishi, N.; Wang, L.; Fan, Z.; Himeda, Y. Heterogeneous Catalysis for Carbon Dioxide Mediated Hydrogen Storage Technology Based on Formic Acid. *Adv. Energy Mater.* **2022**, *12*, 2200817. [\[CrossRef\]](#)
55. Mori, K.; Taga, T.; Yamashita, H. Isolated Single-Atomic Ru Catalyst Bound on a Layered Double Hydroxide for Hydrogenation of CO₂ to Formic Acid. *ACS Catal.* **2017**, *7*, 3147–3151. [\[CrossRef\]](#)
56. Bulut, A.; Yurderi, M.; Karatas, Y.; Say, Z.; Kivrak, H.; Kaya, M.; Gulcan, M.; Ozensoy, E.; Zahmakiran, M. MnO_x-Promoted PdAg Alloy Nanoparticles for the Additive-Free Dehydrogenation of Formic Acid at Room Temperature. *ACS Catal.* **2015**, *5*, 6099–6110. [\[CrossRef\]](#)
57. Karatas, Y.; Bulut, A.; Yurderi, M.; Ertas, I.E.; Alal, O.; Gulcan, M.; Celebi, M.; Kivrak, H.; Kaya, M.; Zahmakiran, M. PdAu-MnO nanoparticles supported on amine-functionalized SiO₂ for the room temperature dehydrogenation of formic acid in the absence of additives. *Appl. Catal. B* **2016**, *180*, 586–595. [\[CrossRef\]](#)
58. Zou, L.; Chen, M.; Zhang, Q.; Mao, Q.; Huang, Y.; Liang, Z. Pd/UIO-66/sepiolite: Toward highly efficient dual-supported Pd-based catalyst for dehydrogenation of formic acid at room temperature. *J. Catal.* **2020**, *388*, 66–76. [\[CrossRef\]](#)
59. Sordakis, K.; Tang, C.; Vogt, L.K.; Junge, H.; Dyson, P.J.; Beller, M.; Laurenczy, G. Homogeneous Catalysis for Sustainable Hydrogen Storage in Formic Acid and Alcohols. *Chem. Rev.* **2018**, *118*, 372–433. [\[CrossRef\]](#)
60. Jantke, D.; Pardatscher, L.; Drees, M.; Cokoja, M.; Herrmann, W.A.; Kuhn, F.E. Hydrogen Production and Storage on a Formic Acid/Bicarbonate Platform using Water-Soluble N-Heterocyclic Carbene Complexes of Late Transition Metals. *ChemSusChem* **2016**, *9*, 2849–2854. [\[CrossRef\]](#)
61. Wang, J.; Jin, H.; Wang, W.H.; Zhao, Y.; Li, Y.; Bao, M. Ultrasmall Ni-ZnO/SiO₂ Synergistic Catalyst for Highly Efficient Hydrogenation of NaHCO₃ to Formic Acid. *ACS Appl. Mater. Interfaces* **2020**, *12*, 19581–19586. [\[CrossRef\]](#)
62. Treigerman, Z.; Sasson, Y. Generation and Quantification of Formate Ion Produced from Aqueous Sodium Bicarbonate in the Presence of Homogeneous Ruthenium Catalyst. *ACS Omega* **2018**, *3*, 12797–12801. [\[CrossRef\]](#)
63. Wang, Q.; Tsumori, N.; Kitta, M.; Xu, Q. Fast Dehydrogenation of Formic Acid over Palladium Nanoparticles Immobilized in Nitrogen-Doped Hierarchically Porous Carbon. *ACS Catal.* **2018**, *8*, 12041–12045. [\[CrossRef\]](#)
64. Lundsted, L.G. The Hydrogenation of Sodium Bicarbonate to Sodium Formate. *J. Am. Chem. Soc.* **1949**, *71*, 323–324. [\[CrossRef\]](#)
65. Xu, F.; Huang, W.; Wang, Y.; Astruc, D.; Liu, X. Efficient and controlled H₂ release from sodium formate. *Inorg. Chem. Front.* **2022**, *9*, 3514–3521. [\[CrossRef\]](#)
66. Xu, F.; Yan, J.; Wang, Y.; Liu, X. Mechanistic insight into efficient H₂ generation upon HCOONa hydrolysis. *iScience* **2023**, *26*, 106504. [\[CrossRef\]](#)
67. Grasmann, M.; Laurenczy, G. Formic acid as a hydrogen source—Recent developments and future trends. *Energy Environ. Sci.* **2012**, *5*, 8171–8181. [\[CrossRef\]](#)
68. Wang, W.H.; Himeda, Y.; Muckerman, J.T.; Manbeck, G.F.; Fujita, E. CO₂ Hydrogenation to Formate and Methanol as an Alternative to Photo- and Electrochemical CO₂ Reduction. *Chem. Rev.* **2015**, *115*, 12936–12973. [\[CrossRef\]](#)
69. Sun, Q.; Wang, N.; Xu, Q.; Yu, J. Nanopore-Supported Metal Nanocatalysts for Efficient Hydrogen Generation from Liquid-Phase Chemical Hydrogen Storage Materials. *Adv. Mater.* **2020**, *32*, 2001818. [\[CrossRef\]](#)
70. Alvarez, A.; Bansode, A.; Urakawa, A.; Bavykina, A.V.; Wezendonk, T.A.; Makkee, M.; Gascon, J.; Kapteijn, F. Challenges in the Greener Production of Formates/Formic Acid, Methanol, and DME by Heterogeneously Catalyzed CO₂ Hydrogenation Processes. *Chem. Rev.* **2017**, *117*, 9804–9838. [\[CrossRef\]](#)
71. Wei, D.; Shi, X.; Qu, R.; Junge, K.; Junge, H.; Beller, M. Toward a Hydrogen Economy: Development of Heterogeneous Catalysts for Chemical Hydrogen Storage and Release Reactions. *ACS Energy Lett.* **2022**, *7*, 3734–3752. [\[CrossRef\]](#)
72. Chatterjee, S.; Dutta, I.; Lum, Y.; Lai, Z.; Huang, K.W. Enabling storage and utilization of low-carbon electricity: Power to formic acid. *Energy Environ. Sci.* **2021**, *14*, 1194–1246. [\[CrossRef\]](#)
73. Asefa, T.; Koh, K.; Yoon, C.W. CO₂-Mediated H₂ Storage-Release with Nanostructured Catalysts: Recent Progresses, Challenges, and Perspectives. *Adv. Energy Mater.* **2019**, *9*, 1901158. [\[CrossRef\]](#)
74. Ji, L.; Cui, T.; Nie, X.; Zheng, Y.; Zheng, X.; Fu, H.; Yuan, M.; Chen, H.; Xu, J.; Li, R. Catalytic hydrogenation of CO₂ with unsymmetric N-heterocyclic carbene–nitrogen–phosphine ruthenium complexes. *Catal. Sci. Technol.* **2021**, *11*, 6965–6969. [\[CrossRef\]](#)

75. Kipshagen, A.; Baums, J.C.; Hartmann, H.; Besmehn, A.; Hausoul, P.J.C.; Palkovits, R. Formic acid as H₂ storage system: Hydrogenation of CO₂ and decomposition of formic acid by solid molecular phosphine catalysts. *Catal. Sci. Technol.* **2022**, *12*, 5649–5656. [\[CrossRef\]](#)
76. Park, K.; Gunasekar, G.H.; Prakash, N.; Jung, K.D.; Yoon, S. A Highly Efficient Heterogenized Iridium Complex for the Catalytic Hydrogenation of Carbon Dioxide to Formate. *ChemSusChem* **2015**, *8*, 3410–3413. [\[CrossRef\]](#)
77. Wang, H.; Chi, Y.; Gao, D.; Wang, Z.; Wang, C.; Wang, L.; Wang, M.; Cheng, D.; Zhang, J.; Wu, C.; et al. Enhancing formic acid dehydrogenation for hydrogen production with the metal/organic interface. *Appl. Catal. B* **2019**, *255*, 117776. [\[CrossRef\]](#)
78. Sun, R.; Liao, Y.; Bai, S.T.; Zheng, M.; Zhou, C.; Zhang, T.; Sels, B.F. Heterogeneous catalysts for CO₂ hydrogenation to formic acid/formate: From nanoscale to single atom. *Energy Environ. Sci.* **2021**, *14*, 1247–1285. [\[CrossRef\]](#)
79. Gunasekar, G.H.; Yoon, S. A phenanthroline-based porous organic polymer for the iridium-catalyzed hydrogenation of carbon dioxide to formate. *J. Mater. Chem. A* **2019**, *7*, 14019–14026. [\[CrossRef\]](#)
80. Gunasekar, G.H.; Shin, J.; Jung, K.D.; Park, K.; Yoon, S. Design Strategy toward Recyclable and Highly Efficient Heterogeneous Catalysts for the Hydrogenation of CO₂ to Formate. *ACS Catal.* **2018**, *8*, 4346–4353. [\[CrossRef\]](#)
81. Shen, Y.; Zhan, Y.; Bai, C.; Ning, F.; Wang, H.; Wei, J.; Lv, G.; Zhou, X. Immobilized iridium complexes for hydrogen evolution from formic acid dehydrogenation. *Sustain. Energy Fuels* **2020**, *4*, 2519–2526. [\[CrossRef\]](#)
82. Wang, C.; Wang, Z.; Mao, S.; Chen, Z.; Wang, Y. Coordination environment of active sites and their effect on catalytic performance of heterogeneous catalysts. *Chin. J. Catal.* **2022**, *43*, 928–955. [\[CrossRef\]](#)
83. Zaidman, B.; Wiener, H.; Sasson, Y. Formate salts as chemical carriers in hydrogen storage and transportation. *Int. J. Hydrogen Energy* **1986**, *11*, 341–347. [\[CrossRef\]](#)
84. Wiener, H.; Zaidman, B.; Sasson, Y. Storage of energy by solutions of alkali formate salts. *Sol. Energy* **1989**, *43*, 291–296. [\[CrossRef\]](#)
85. Su, J.; Yang, L.; Lu, M.; Lin, H. Highly efficient hydrogen storage system based on ammonium bicarbonate/formate redox equilibrium over palladium nanocatalysts. *ChemSusChem* **2015**, *8*, 813–816. [\[CrossRef\]](#)
86. Lu, M.; Zhang, J.; Yao, Y.; Sun, J.; Wang, Y.; Lin, H. Renewable energy storage via efficient reversible hydrogenation of piperidine captured CO₂. *Green Chem.* **2018**, *20*, 4292–4298. [\[CrossRef\]](#)
87. Bi, Q.Y.; Lin, J.D.; Liu, Y.M.; He, H.Y.; Huang, F.Q.; Cao, Y. Dehydrogenation of Formic Acid at Room Temperature: Boosting Palladium Nanoparticle Efficiency by Coupling with Pyridinic-Nitrogen-Doped Carbon. *Angew. Chem. Int. Ed.* **2016**, *55*, 11849–11853. [\[CrossRef\]](#) [\[PubMed\]](#)
88. Wang, F.; Xu, J.; Shao, X.; Su, X.; Huang, Y.; Zhang, T. Palladium on Nitrogen-Doped Mesoporous Carbon: A Bifunctional Catalyst for Formate-Based, Carbon-Neutral Hydrogen Storage. *ChemSusChem* **2016**, *9*, 246–251. [\[CrossRef\]](#)
89. Koh, K.; Jeon, M.; Chevrier, D.M.; Zhang, P.; Yoon, C.W.; Asefa, T. Novel nanoporous N-doped carbon-supported ultrasmall Pd nanoparticles: Efficient catalysts for hydrogen storage and release. *Appl. Catal. B* **2017**, *203*, 820–828. [\[CrossRef\]](#)
90. Shao, X.; Miao, X.; Zhang, T.; Wang, W.; Wang, J.; Ji, X. Pd Nanoparticles Supported on N- and P-Co-doped Carbon as Catalysts for Reversible Formate-Based Chemical Hydrogen Storage. *ACS Appl. Nano Mater.* **2020**, *3*, 9209–9217. [\[CrossRef\]](#)
91. Bi, Q.Y.; Lin, J.D.; Liu, Y.M.; Du, X.L.; Wang, J.Q.; He, H.Y.; Cao, Y. An aqueous rechargeable formate-based hydrogen battery driven by heterogeneous Pd catalysis. *Angew. Chem. Int. Ed.* **2014**, *53*, 13583–13587. [\[CrossRef\]](#) [\[PubMed\]](#)
92. Shin, D.Y.; Kim, M.S.; Kwon, J.A.; Shin, Y.J.; Yoon, C.W.; Lim, D.H. Fundamental Mechanisms of Reversible Dehydrogenation of Formate on N-Doped Graphene-Supported Pd Nanoparticles. *J. Phys. Chem. C* **2018**, *123*, 1539–1549. [\[CrossRef\]](#)
93. Lee, J.H.; Ryu, J.; Kim, J.Y.; Nam, S.W.; Han, J.H.; Lim, T.H.; Gautam, S.; Chae, K.H.; Yoon, C.W. Carbon dioxide mediated, reversible chemical hydrogen storage using a Pd nanocatalyst supported on mesoporous graphitic carbon nitride. *J. Mater. Chem. A* **2014**, *2*, 9490–9495. [\[CrossRef\]](#)
94. Shao, X.; Xu, J.; Huang, Y.; Su, X.; Duan, H.; Wang, X.; Zhang, T. Pd@C₃N₄ nanocatalyst for highly efficient hydrogen storage system based on potassium bicarbonate/formate. *AIChE J.* **2016**, *62*, 2410–2418. [\[CrossRef\]](#)
95. Mori, K.; Masuda, S.; Tanaka, H.; Yoshizawa, K.; Che, M.; Yamashita, H. Phenylamine-functionalized mesoporous silica supported PdAg nanoparticles: A dual heterogeneous catalyst for formic acid/CO₂-mediated chemical hydrogen delivery/storage. *Chem. Commun.* **2017**, *53*, 4677–4680. [\[CrossRef\]](#) [\[PubMed\]](#)
96. Sun, Q.; Chen, B.W.J.; Wang, N.; He, Q.; Chang, A.; Yang, C.M.; Asakura, H.; Tanaka, T.; Hulsey, M.J.; Wang, C.H.; et al. Zeolite-Encaged Pd-Mn Nanocatalysts for CO₂ Hydrogenation and Formic Acid Dehydrogenation. *Angew. Chem. Int. Ed.* **2020**, *59*, 20183–20191. [\[CrossRef\]](#)
97. Nakajima, K.; Tominaga, M.; Waseda, M.; Miura, H.; Shishido, T. Highly Efficient Supported Palladium–Gold Alloy Catalysts for Hydrogen Storage Based on Ammonium Bicarbonate/Formate Redox Cycle. *ACS Sustain. Chem. Eng.* **2019**, *7*, 6522–6530. [\[CrossRef\]](#)
98. Zou, L.; Liu, Q.; Zhang, Q.; Zhu, Z.; Huang, Y.; Liang, Z. Synthesis of Bimetallic Pd-Based/Activated Carbon Catalyst by Biomass-Reduction Method for Highly Efficient Hydrogen Storage System Based on CO₂/Formate. *Ind. Eng. Chem. Res.* **2022**, *61*, 2455–2468. [\[CrossRef\]](#)
99. Jiang, S.; Yang, J.; Zhai, S.; Zhang, L.; Tu, R.; Yu, T.; Zhai, D.; Sun, L.; Deng, W.; Ren, G. Ambient Hydrogen Storage and Release Using CO₂ and an L-Arginine-Functionalized PdAu Catalyst via pH Control. *ACS Catal.* **2022**, *12*, 14113–14122. [\[CrossRef\]](#)
100. Masuda, S.; Mori, K.; Futamura, Y.; Yamashita, H. PdAg Nanoparticles Supported on Functionalized Mesoporous Carbon: Promotional Effect of Surface Amine Groups in Reversible Hydrogen Delivery/Storage Mediated by Formic Acid/CO₂. *ACS Catal.* **2018**, *8*, 2277–2285. [\[CrossRef\]](#)

101. Zhong, H.; Iguchi, M.; Chatterjee, M.; Ishizaka, T.; Kitta, M.; Xu, Q.; Kawanami, H. Interconversion between CO₂ and HCOOH under Basic Conditions Catalyzed by PdAu Nanoparticles Supported by Amine-Functionalized Reduced Graphene Oxide as a Dual Catalyst. *ACS Catal.* **2018**, *8*, 5355–5362. [[CrossRef](#)]
102. Masuda, S.; Shimoji, Y.; Mori, K.; Kuwahara, Y.; Yamashita, H. Interconversion of Formate/Bicarbonate for Hydrogen Storage/Release: Improved Activity Following Sacrificial Surface Modification of a Ag@Pd/TiO₂ Catalyst with a TiO_x Shell. *ACS Appl. Energy Mater.* **2020**, *3*, 5819–5829. [[CrossRef](#)]

Disclaimer/Publisher's Note: The statements, opinions and data contained in all publications are solely those of the individual author(s) and contributor(s) and not of MDPI and/or the editor(s). MDPI and/or the editor(s) disclaim responsibility for any injury to people or property resulting from any ideas, methods, instructions or products referred to in the content.